JACS
JOURNAL OF THE AMERICAN CHEMICAL SOCIETY
Article
pubs.acs.org/JACS

Trapped State Sensitive Kinetics in $LaTiO_2N$ Solid Photocatalyst with and without Cocatalyst Loading

Rupashree Balia Singh,[†] Hiroyuki Matsuzaki,[†] Yohichi Suzuki,[†,‡] Kazuhiko Seki,[†] Tsutomu Minegishi,[‡,§] Takashi Hisatomi,[‡,§] Kazunari Domen,*[,‡,§] and Akihiro Furube*[,†]

[†]National Institute of Advanced Industrial Science and Technology (AIST), Tsukuba Central 5, 1-1-1 Higashi, Tsukuba, Ibaraki 305-8565, Japan

[‡]Department of Chemical System Engineering, The University of Tokyo, 7-3-1 Hongo, Bunkyo-ku, Tokyo 113-8656, Japan

[§]Japan Technological Research Association of Artificial Photosynthetic Chemical Process (ARPChem), 5-1-5 Kashiwanoha, Kashiwa, Chiba 277-8589, Japan

Supporting Information

ABSTRACT: In addition to the process of photogeneration of electrons and holes in photocatalyst materials, the competitive process of trapping of these charge carriers by existing defects, which can both enhance the photocatalytic activity by promoting electron−hole separation or can deteriorate the activity by serving as recombination centers, is also very crucial to the overall performance of the photocatalyst. In this work, using femtosecond diffuse reflectance spectroscopy we have provided evidence for the existence of energetically distributed trapped states in visible-light responsive solid photocatalyst powder material $LaTiO_2N$ (LTON). We observe trapped state sensitive kinetics in bare-LTON. CoO_x cocatalyst loading (2 wt % CoO_x-LTON) shows effect on the kinetics only when presence of excess energy (for above bandgap excitation) results in the generation of surface carriers. Thus, the kinetics show appreciable excitation wavelength dependence, and the experimental results obtained for different λ_{exc} have been rationalized on this basis. In an earlier work by Domen and co-workers, the optimized CoO_x/LTON has been reported to exhibit a high quantum efficiency of 27.1 ± 2.6% at 440 nm, the highest reported for this class of photocatalysts (*J. Am. Chem. Soc.* **2012**, *134*, 8348−8351). In the present work, the mechanism is addressed in terms of picosecond charge carrier dynamics.

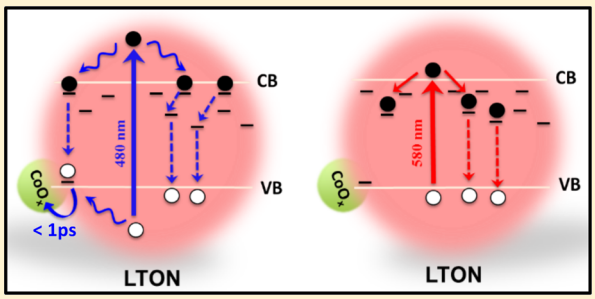

INTRODUCTION

With increasing energy needs of the global population and depleting sources of fossil fuels, the world is currently searching for inexpensive alternative forms of energy that are clean, recyclable and transportable. In recent times, hydrogen produced from water using renewable solar energy has come up as a promising next-generation fuel.[1,2] Over the past decades, the photocatalytic water-splitting reaction using semiconductors as both the light absorber and energy converter has been studied to store solar energy in the simplest chemical bond, H_2.[3,4] In recent times, a lot of effort is being put into the design and synthesis of materials with a narrow band gap to efficiently harvest the visible light photons, which comprise ∼47% of the solar spectrum, but this in turn decreases the driving force for the water oxidation−reduction reactions.[5,6] The achievable theoretical potential of a photocatalyst with a visible light absorption edge of 600 nm (bandgap of 2.1 eV) is 16.2% solar-energy-conversion efficiency (assuming an overall water splitting quantum yield of unity).[5] Thus, the development of this "600 nm-class photocatalysts" is crucial for the overall improvement in solar energy conversion.

The oxynitride $LaTiO_2N$ (LTON) is an n-type semiconductor material with a perovskite structure and a band gap of 2.1 eV (∼600 nm absorption edge).[7−9] In presence of suitable sacrificial reagents and cocatalysts, LTON has been reported to exhibit the ability to generate H_2 and O_2 from water under irradiation of light with wavelengths up to 600 nm.[10,11] However, presence of a considerable number of defects that cause trapping and recombination of photoexcited carriers limits its photoactivity.[12]

Efficient conversion using solar energy requires precise fine-tuning of not only the composition and structure of the materials but also the thermodynamic and kinetic aspects of the carrier dynamics.[13] Transient absorption spectroscopy (TAS) serves as a very useful tool in monitoring the carrier dynamics in photocatalytic systems and has successfully revealed the trapping and recombination kinetics of photogenerated electrons and holes in the most widely used semiconductor photocatalyst TiO_2.[14−17] The spectral features over a wide wavelength range have been successfully assigned to trapped

Received: October 7, 2014
Published: November 14, 2014

   dx.doi.org/10.1021/ja5102823 | *J. Am. Chem. Soc.* 2014, 136, 17324−17331

electrons and holes and to free bulk carriers in nanocrystalline TiO_2 films and their time evolution is also estimated.[14−17] A variety of other photocatalytic systems such as GaN:ZnO, $LaAlO_3/SrTiO_3$ heterostructures, α-Fe_2O_3 etc.[18−23] and also some very innovative photocatalytic materials such as three-dimensional CdS-Titanate nanocomposites[24] and Ag@AgCl cubic cages[25] have also been successfully investigated using TAS. In general, the complicated carrier dynamics needs monitoring of a wide spectral and temporal window to gain a better insight into the whole process. Photogeneration, thermal relaxation, trapping, recombination and interfacial charge transfers mostly occur on femtosecond to picosecond time scales.[13] Thus, understanding the carrier dynamics in the early stages is crucial to the understanding of the overall performance of the photocatalytic material.[13,14,21−25]

For materials, which are translucent or opaque, instead of transmitted light as done in case of TAS, the diffuse reflected light from the sample can be effectively collected and analyzed to obtain similar information on the kinetics of transient species.[26−28] In this work, we use femtosecond and subnanosecond time-resolved diffuse reflectance (fs-TRDR and sub-ns-TRDR) spectroscopy to elucidate the complicated carrier dynamics in n-type perovskite semiconductor photocatalyst LTON. TRDR serves as a very useful tool in monitoring the carrier dynamics in such opaque powder photocatalyst systems and it has been successfully applied to TiO_2 powders. Recently, Yamanaka et al.[27,28] studied carrier dynamics in Nitrogen-doped TiO_2 powders using femtosecond TRDR spectroscopy. In this paper, the trapped state sensitive kinetics in bare-LTON and 2 wt % CoO_x-LTON is rationalized in terms of the variation in the distribution of photogenerated carriers in an energetic distribution of traps in the material which in turn gives rise to an excitation wavelength dependent kinetics. As already mentioned in the abstract, the optimized CoO_x/LTON has been reported to exhibit a high quantum efficiency of 27.1 ± 2.6% at 440 nm, the highest reported for this class of photocatalysts.[10] Since the first report by Kanan and Nocera et al.[29] that Co based materials such as Co-Pi and CoO_x can serve as electrocatalysts, they have found wide applications in photoelectrodes and photocatalysts.

EXPERIMENTAL SECTION

Sample Preparation. $La_2Ti_2O_7$ was prepared as a starting material for $LaTiO_2N$. La_2O_3 (99.99%, Kanto), which was freshly calcined at 1273 K for 10 h to remove carbonates and hydroxides, and rutile-type TiO_2 (99.99%, Aldrich) were mixed using an alumina mortar. Subsequently, NaCl (99.5%, Wako) was added to the mixture and ground for 1 h. The molar ratio of the starting materials was La_2O_3:TiO_2:NaCl = 1:2:20. The mixture was heated to 1423 K at the rate of 10 K min^{-1} in alumina crucibles, held at the target temperature for 5 h, cooled to 1073 K at the rate of 1 K min^{-1}, and finally allowed to be cooled to room temperature naturally. The product mass was stirred in 500 mL of distilled water and collected by sedimentation five times, filtrated with addition of a sufficient amount of water, and dried at 343 K. The yield of the $La_2Ti_2O_7$ product was 98%. The obtained $La_2Ti_2O_7$ was nitrided to $LaTiO_2N$ under an NH_3 flow (Sumitomo, 99.9995%) of 250 mL min^{-1} at 1223 K for 4 h. The CoO_x catalyst (2 wt % Co with respect to $LaTiO_2N$) was loaded by impregnation from an aqueous $Co(NO_3)_2$ solution followed by a heat treatment at 823 K for 1 h under an NH_3 flow (50 mL min^{-1}). Finally, the sample was heated in air at 473 K for 1 h.

Instrumental Details. Steady state diffuse reflectance measurements were carried out with an absorption spectrophotometer (Shimadzu, UV-3101PC). Absorption spectra for ground state were estimated using the Kubelka−Munk function:[14]

$$\frac{K}{S} = \frac{(1-R)^2}{2R} \quad (1)$$

where K and S are the absorption and scattering coefficients, respectively, and R is the diffuse reflectance.

The detailed description of the fs-TRDR setup is provided elsewhere.[17] Briefly, for fs-TRDR spectroscopy, fundamental beam from a femtosecond Ti:sapphire laser with a regenerative amplifier (Hurricane, Spectra Physics, 800 nm, 130 fs, 1 mJ/pulse, 1 kHz) is used. Coupled with an optical parametric amplifier (OPA) (TOPAS, Quantronix), the fundamental is used to generate the pump pulses at 480 or 580 nm. The instrument response for both pump wavelengths is <1 ps. The powder samples are taken in 1 mm quartz cuvettes. The pump beam diameter on the sample surface was about 0.5 mm as observed with a CCD camera. The probe beam was a white light continuum generated by focusing a part of the fundamental from the Ti-Sapphire laser into a sapphire plate (450−1200 nm). To probe IR wavelength (3440 nm), differential frequency generation method of the OPA was used. Amplified Si photodetector, an InGaAs photodetector, or a mercury−cadmium-telluride (MCT) photodetector were used depending on the probe wavelengths monitored (400−1000, 800−1500 and 1500−5000 nm, respectively) and the diffuse reflected probe beam was then detected after passing through a grating monochromator (Acton Research, SpectraPro-150). All measurements were performed in air at room temperature and under weak excitation conditions (at a pump power of 0.3 μJ) to rule out the influence of second-order electron−hole recombination. The transient absorption intensity of the TRDR spectrum is presented as percentage absorption, where % absorption = $100(1 - R/R_0)$, where R and R_0 are the intensities of the diffuse reflected light with and without excitation, respectively.[26] Hereafter, in the manuscript TRDR spectrum is sometimes interchanged with the term transient absorption spectrum (TAS) as the linearity between % absorption and the concentration of transient species is maintained for % absorption values below 10%.[26]

Nanosecond TRDR measurements were carried out using the second harmonic (532 nm, 10 Hz, ∼150 ps) of a Nd^{3+}:YAG laser (Ekspla, SL311) after pulse compression as the excitation source.[30] The powder samples are taken in 1 mm quartz cuvettes. The pump beam diameter on the sample surface was about 6 mm. A xenon flash lamp (Hamamatsu, L4642, ∼2 μs pulse duration) was used as the probe white light source. The time resolution of the setup was roughly <1 ns. No monochromator was used, instead the total diffuse reflected light from the sample in the NIR region (900−1500 nm) was introduced into an InGaAs photodiode (New Focus, 1601) after passing through an 800 nm cutoff filter. This method was employed in order to improve the signal strength, which was otherwise weak if single wavelengths were monitored. The signal from the detector was then introduced into a digital oscilloscope (LeCroy, 6200A). An averaging over 200 shots was done for each measurement to improve signal quality. Five such measurements were averaged to obtain the final displayed data. The intensity of the pump pulse was measured using a pyroelectric energy meter (OPHIR, PE25-SH-V2) and power adjustments were done to make the nanosecond data compatible with the picosecond data. Measurements were performed in air at room temperature.

RESULTS AND DISCUSSION

Steady State Absorption and Characterization of LTON Samples. Figure 1a shows the Kubelka−Munk absorption profiles of bare and 2 wt % CoO_x loaded LTON powders. The absorption edge for both the samples is around 600 nm as is expected from this "600 nm-class photocatalyst". The background absorption above 600 nm edge for LTON is usually attributed to Ti^{3+} reduced species or anion vacancies introduced during the preparatory steps of the material which could serve as charge recombination centers.[12] The excitation wavelengths for fs-TRDR studies are selected at 480 nm (above

dx.doi.org/10.1021/ja5102823 | J. Am. Chem. Soc. 2014, 136, 17324−17331

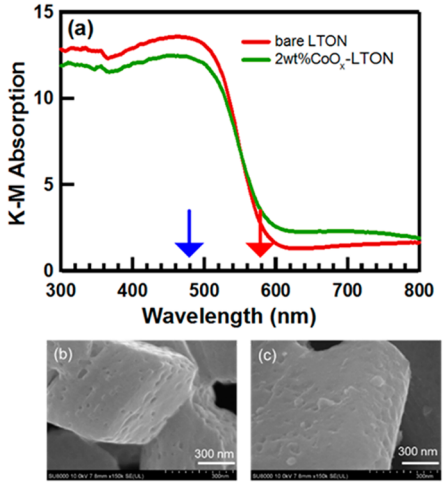

Figure 1. (a) Kubelka–Munk absorption profile (colored arrows indicate the selected excitation wavelengths of 480 and 580 nm). (b) and (c) SEM images of bare-LTON and 2 wt % CoO_x-LTON, respectively.

bandgap excitation) and 580 nm (near bandgap excitation) for comparison of carrier kinetics. As is evident from Figure 1a, there is a large difference in the absorption coefficients at the two excitation wavelengths. Another point to mention here is that the steady state diffuse reflectance values (Figure not shown) observed for both the samples at 480 nm are almost the same, and hence, the light absorption by LTON seems to remain unaffected due to cocatalyst loading, i.e., there is no shading due to cocatalyst. But, at 580 nm, 2 wt % cocatalyst loading results in nearly 20% higher absorption. This background absorption further increases with higher CoO_x loading (Figure not shown) hinting at some kind of contribution from Co species. This results in reduced light absorption by the actual LTON sample when excited at 580 nm which is addressed in more details in the later sections. The SEM image of bare-LTON (Figure 1b) shows brick-like LTON particles with a porous structure and the surface of the particles was mostly smooth with particle size roughly in the range of 1 μm. SEM image of 2 wt % CoO_x-LTON show attached nanoparticles of the cocatalyst on the surface of LTON. Mostly the CoO_x particles are of 10 nm size, though some larger aggregates are also obvious from the image.

fs-TRDR Spectra. As mentioned earlier, the optimized CoO_x/LTON has been reported to exhibit a high quantum efficiency of 27.1 ± 2.6% at 440 nm and the lifetime of the excited electrons (λ_{exc} = 355 nm 1 mJ UV pulse) are prolonged in the time scale of 1 s.[10] Apart from this work, very recently Yamakata et al.[31] reported the effect of CoO_x and Pt loading on the behavior of photogenerated carriers in LTON using femtosecond to second time-resolved visible to mid-IR absorption spectroscopy primarily under 355 nm UV pulse excitation similar to that used in ref 10. Though their picosecond measurements were done under 500 nm excitation, but the intensity of the pump pulse used made second-order recombination inevitable. They did observe a dependence of decay on the intensity of the pump pulse in the picosecond regime. Ruling out second order recombination is an important criterion for accurate elucidation of the actual reaction mechanism. In our work, we have greatly improved the measurement conditions and have tried to work under weak excitations so that as far as possible we could correlate the transient absorption spectroscopy results with the photocatalytic reaction under practical conditions. We also strongly felt that the scenario could be very different when looking at the early carrier dynamics where excitation energy might play a decisive role in determining the carrier migration. Thus, in the present work, we deliberately chose to excite the LTON samples at two different wavelengths: at 480 nm (above bandgap excitation) and 580 nm (near bandgap excitation) in order to do a systematic analysis of the role of excess energy on the charge carrier dynamics in the ps-regime and its impact on the effect of CoO_x loading on LTON powder.

Figure 2 shows the fs-TRDR spectra under weak excitation condition (see Figure S1 for excitation intensity dependence) at

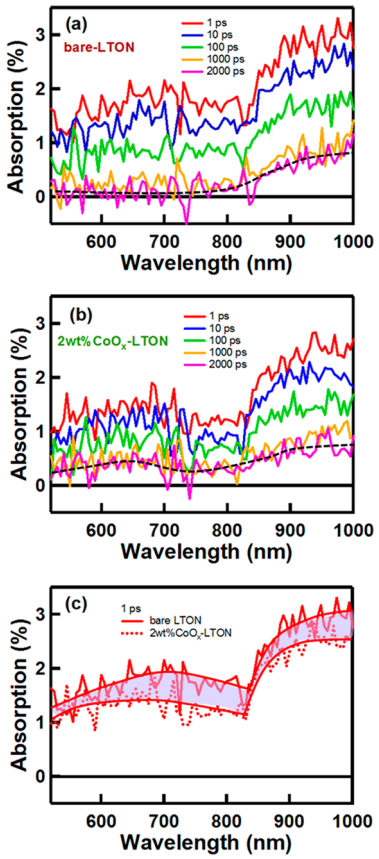

Figure 2. Transient absorption spectrum at different delay times after excitation (λ_{exc} = 480 nm, pump energy = 0.3 μJ) for (a) bare-LTON, (b) 2 wt % CoO_x-LTON and (c) depicts the drop in signal strength on CoO_x loading on LTON corresponding to hole scavenging in <1 ps after excitation.

different time delays up to 2 ns after excitation for both bare-LTON and 2 wt % CoO_x-LTON for λ_{exc} = 480 nm. For our measurements, the zero delay time (i.e., time zero) corresponds to ~3 ps on the time axis so, the times depicted in Figure 2 and hereafter are actually delay times after excitation (i.e., after time zero). As is evident from the figures, the spectral profiles are broad, ranging from 530 to 1000 nm and look almost similar for both the materials. However, their decay dynamics differs significantly (see Figure S2 for the fs-TRDR spectra beyond 1000 nm). Comparing Figure 2a and b, we can see that the initial TA intensity (at 1 ps after excitation) is lower for 2 wt % CoO_x-LTON under similar experimental conditions. In order to make the differences for the two materials more explicit, in

dx.doi.org/10.1021/ja5102823 | J. Am. Chem. Soc. 2014, 136, 17324–17331

Figure 2c we try to compare the spectrum at 1 ps after excitation for both the materials The shaded region in Figure 2c corresponds to the difference in the TA intensities for the two materials over the measured spectral range which appears as a broad absorption spanning over the whole range. This initial drop in TA intensity for 2 wt % CoO_x-LTON is attributed to the scavenging of surface holes by the oxidation cocatalyst CoO_x within the time resolution of our instrumental setup (i.e., in <1 ps). Similarly at later times, i.e., at 2 ns after excitation, we observe that the TAS for bare-LTON and 2 wt % CoO_x-LTON look significantly different especially in the region below 800 nm (spectra highlighted by dotted lines in Figure 2a and b). There still remains an appreciable signal strength for 2 wt % CoO_x-LTON, whereas for bare-LTON, the signal has gone down to almost zero. This gives the first hint at the appearance of the TA signal for different photogenerated carriers at different spectral regions. However, precisely distinguishing the contributions from different species in this broad spectrum is difficult. But, broadly for the purpose of comparison we can divide the transient absorption spectrum into two regions, i.e., above and below 800 nm and select two probe wavelengths (650 and 920 nm) for comparison of kinetics.

The decay kinetics monitored at 650 and 920 nm for bare-LTON and 2 wt % CoO_x-LTON are shown in Figure 3a and b.

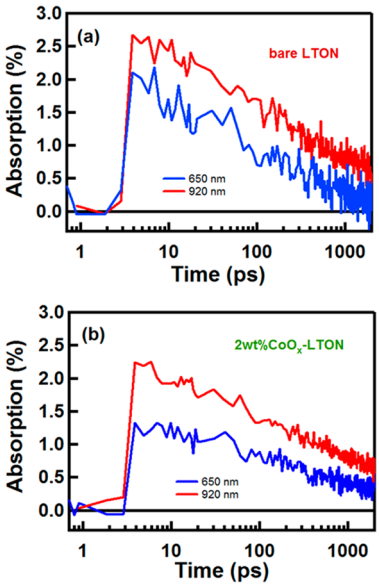

Figure 3. Comparison of femtosecond time profiles (λ_{exc} = 480 nm, pump energy = 0.3 μJ) for (a) bare-LTON and (b) 2 wt % CoO_x-LTON monitored at 650 and 920 nm.

A rough estimate of the average time in which the population of the photogenerated species at any particular probe wavelength is reduced to half its number ($t_{1/2}$) helps us understand the difference more explicitly even though $t_{1/2}$ has no such physical relevance.[22] The approximate values of $t_{1/2}$ and the percentage of surviving carriers at 2 ns after excitation are given in Table 1. The major difference that is obvious from the figures and the values of $t_{1/2}$ in Table 1 is the faster decay for 650 nm time profile in case of bare-LTON ($t_{1/2}$ = 70 ps) compared to the same in 2 wt % CoO_x-LTON ($t_{1/2}$ = 320 ps). Similarly, the estimated percentage of surviving carriers at 2 ns also point to the fact that whereas ~28% carriers survive for 2 wt % CoO_x-LTON, the number is negligible for bare-LTON (<10% within

Table 1. Estimated Values of $t_{1/2}$ and Percentage of Surviving Carriers at 650/700 and 920 nm Probe Wavelengths for Bare-LTON and 2 wt % CoO_x-LTON (λ_{exc} = 480 nm)[a]

	$t_{1/2}$		% age of surviving carriers (at 2 ns)	
samples	650/700 nm	920 nm	650/700 nm	920 nm
bare-LTON	70 ps (1.5 ns)	270 ps (1.8 ns)	<10 (~50)	27 (~50)
2 wt % CoO_x-LTON	320 ps (1.6 ns)	310 ps (1.8 ns)	28 (~50)	29 (~50)

[a]The values in parentheses are for λ_{exc} = 580 nm.

error limit). This brings us to the conclusion that the 650 nm decay profile is affected significantly on CoO_x loading. These observations enable us to unambiguously assign the spectral position of 650 nm to an overlapping contribution from both surface trapped electrons and holes. In presence of CoO_x, due to scavenging of surface holes within time resolution, the surface electrons tends to survive the loss due to electron−hole recombination which is prevalent in bare-LTON, where the 650 nm time profile decays almost completely within 2 ns (Figure 3a). Since 920 nm decay profile remains unaffected by cocatalyst loading, this spectral position is assigned to bulk carriers (both trapped and free carriers). These assignments are further confirmed using methanol (MeOH) as the hole scavenger for bare-LTON (see Figure S3). And as expected, the decay kinetics for free bulk carriers probed in the IR (3440 nm) shows no effect of CoO_x loading (see Figure S4).

As already mentioned in the Introduction section, this work aims at a systematic analysis on how the effect of CoO_x loading is dependent on the choice of the excitation wavelength which could reflect the existence of energetic and spatial distribution of traps in LTON. After obtaining and analyzing the results for λ_{exc} = 480 nm, we then excited the samples at 580 nm to draw a comparative picture. We must mention here that for λ_{exc} = 580 nm, instead of 650 nm we monitored the decay of surface trapped carriers at 700 nm to avoid excessive interference from scattered excitation light entering the detector. We do not expect the kinetics to differ drastically for these two probe wavelengths and hence, for the purpose of comparison this seems reasonable. The results obtained are shown in Figure 4 (some data are the same as in Figure 3 but, plotted differently for easy comparison), where we try to present a comparison of the decay profiles of the two samples (bare-LTON and 2 wt % CoO_x-LTON) at two different probe wavelengths (650/700 and 920 nm) for two different excitation wavelengths (λ_{exc} = 480 and 580 nm). For purpose of clarity, we mention here that from henceforth in the manuscript "650/700 nm" means the surface carriers probed at either 650 or 700 nm; the probe wavelength is 650 nm for λ_{exc} = 480 and 700 nm for λ_{exc} = 580 nm. Figure 4a shows the comparison of the decay profiles at 650/700 nm for bare-LTON and 2 wt % CoO_x-LTON for λ_{exc} 480 and 580 nm. From the corresponding normalized data shown in Figure 4b, it is evident that for λ_{exc} = 580 nm, the two samples show similar decay kinetics, but for λ_{exc} = 480 nm, 2 wt % CoO_x-LTON shows a slower decay (see also Table 1). A similar comparison of the time traces for 920 nm (Figure 4c and d) shows similar kinetics for both the samples for both excitation wavelengths. However, as is obvious from the figures even though both bare-LTON and 2 wt % CoO_x-LTON exhibit similar kinetics for λ_{exc} = 580 nm (at both 700 and 920 nm probe wavelengths), the decay is slower when compared to

dx.doi.org/10.1021/ja5102823 | J. Am. Chem. Soc. 2014, 136, 17324−17331

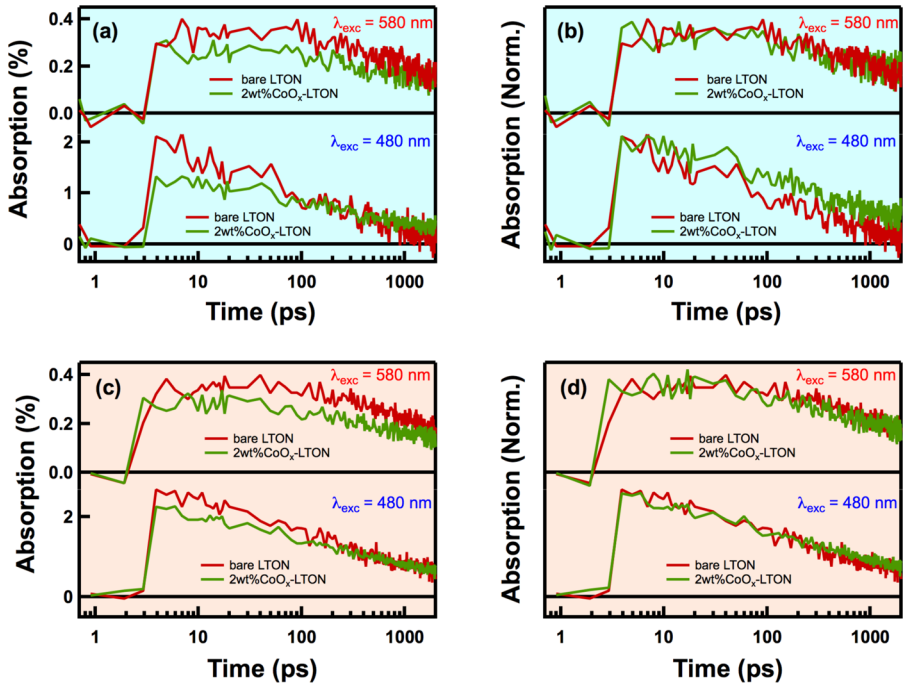

Figure 4. Comparison of femtosecond time profiles for bare-LTON and 2 wt % CoO_x-LTON monitored at (left panel) 650/700 nm and (right panel) 920 nm (λ_{exc} = 480 and 580 nm). (b) and (d) show the normalized data corresponding to (a) and (c), respectively.

their respective counterparts for λ_{exc} = 480 nm. A rough estimate of $t_{1/2}$ values for both the probe wavelengths for λ_{exc} = 580 nm comes out to be more than 1 ns which is significantly higher compared to that obtained for λ_{exc} = 480 (see Table 1). A minor point which needs a quick mention here is the slightly smaller amplitude of TA (λ_{exc} = 580 nm) for 2 wt % CoO_x-LTON compared to bare-LTON for both the probe wavelengths (Figure 4a and c). This can be attributed possibly to slightly lower photon absorption by the actual sample when excited near the band edge where the contribution from background absorption appears higher due to Co loading (Figure 1a). In fact, it has been observed that further Co loading increased this background absorption further (Figure not shown) hinting at some kind of contribution from Co species.

Thus, to sum up the observations we can say the following: (1) Excitation near the band edge, i.e., at 580 nm, results in slowing down of the carrier decay. (2) CoO_x loading on LTON shows an effect on carrier kinetics probed at 650/700 nm only when excited at 480 nm.

In order to rationalize these observations we propose the model depicted in Scheme 1. First, we propose the presence of two types of photogenerated carriers detectable in the vis-NIR region in both samples upon excitation: (1) surface trapped electrons and holes (appearing predominantly below 800 nm in the TAS), and (2) bulk carriers (in the NIR region). As mentioned earlier the free bulk carriers appear predominantly in the IR. Since the light penetration depth at both excitation wavelengths is estimated to be in the order of several microns, we expect a uniform generation of carriers over the surface and bulk of the LTON upon photoexcitation. It is however difficult to spectrally distinguish the species precisely as we observe a broad TAS hinting at overlapping contributions from the above-mentioned species. Second, we assign the decay of the carrier population to both loss due to e-h recombination and relaxation of shallow trapped carriers into deeper traps.

Scheme 1. Schematic Illustration of the Spatial and Energetic Distribution of Electrons and Holes in Bare-LTON and 2 wt % CoO_x-LTON after Excitation at 480 nm (Indicated in Blue)[a] and 580 nm (Indicated in Red)

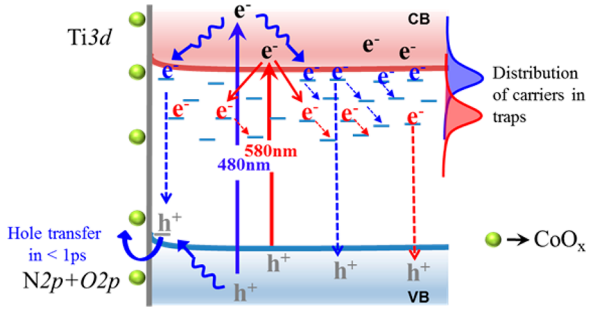

[a]Long dotted arrows indicate e−h recombination and short dotted arrows indicate relaxation of carriers into deeper traps.

Unfortunately, we cannot distinguish the individual contributions from each of the loss channels. For λ_{exc} = 480 nm (above bandgap excitation), the excess energy in the hot photogenerated carriers takes more time to dissipate in the lattice, i.e., for intraband cooling (indicated by blue curved arrows in Scheme 1) before being shallowly trapped near the conduction band (CB) edge. Nozik et al.[32] and Tamaki et al.[17] in separate works have efficiently demonstrated that carriers having larger excess energy in the conduction band needed more time to thermalize and lose this energy before trapping. A similar explanation can be arguably put forward in the present case too. Whereas, for λ_{exc} = 580 nm (near bandgap excitation), there is no such cooling time involved. Direct excitation takes place to the CB edge or possibly even to some shallow traps immediately below the CB. Because of longer instrument response time we are unable to observe the initial cooling and trapping processes. Thus, as is evident from the fs-TAS, for λ_{exc}

dx.doi.org/10.1021/ja5102823 | J. Am. Chem. Soc. 2014, 136, 17324−17331

= 480 nm, at 1 ps after excitation, most of the carriers have thermalized and are shallowly trapped as cooling time was longer but, for λ_{exc} = 580 nm, the carriers within the same time have possibly populated deeper traps. The slower decay ($t_{1/2}$ > 1 ns) for time traces of 700 and 920 nm for λ_{exc} = 580 nm can be best explained in terms of a greater distribution of carriers in deeper traps as compared to when excited at 480 nm (Scheme 1). As we know from literature, more deeply trapped carriers are relatively less mobile than shallow trapped ones and hence, the slowing down of the decay for λ_{exc} = 580 nm is an indication deeper trapping.[13,17,32] Tamaki et al.[17] reported that such deep trapping in TiO_2 nanoparticles results in immobile carriers and this lack of mobility is then the primary reason for the observed microsecond lifetimes of carriers. Thus, deep trapping could also be beneficial for the enhancement of the photocatalytic activity of materials.

Apart from the distribution of carriers into deeper traps, for λ_{exc} = 580 nm, cocatalyst loading has no effect on the resulting carrier dynamics hinting at the absence of the surface carriers in the measured time regime. Presence of excess excitation energy for λ_{exc} = 480 nm could result in the generation of holes lower in the valence band (Scheme 1). These energetic holes can then migrate quickly to surface traps. Matsukawa et al.[12] confirmed the presence of surface traps in LTON, comprising of reduced Ti^{3+} species and nitrogen defects using atomic-resolution scanning transmission electron microscopy and electron energy-loss spectroscopy. They also concluded that for the high photocatalytic activity of LTON it is essential to form reduced Ti^{3+}- including surface regions. On the other hand, for λ_{exc} = 580 nm, the holes are generated close to valence band (VB) edge, possibly in some localized defects (or impurity level) which exist near the edge and this hinders their movement toward the effective surface traps within the time scale of our measurement. However, currently this is just speculative as we have no evidence for the existence of such impurity levels. But, again as we mentioned above, such trapping could also facilitate enhancement of the survival lifetime of the carriers.

Sub-ns-TRDR Spectra and Theoretical Analysis. In order to extend our investigations into the longer delay times (beyond 2 ns), we also measured the carrier dynamics in the nanosecond regime. For this, we excited the bare-LTON powder at 532 nm and collected and analyzed the complete diffuse reflected light in the NIR region (900−1500 nm) (details of the measurement are mentioned in the Instrumental Details section). The observed decay extends from ps to sub-microsecond time range. The decay of bulk carriers by thermal relaxation could be over in subnanosecond time range but the slower decay in the nanosecond time regime is due to the recombination of positive and negative carriers with small rates by tunnelling. Since the experiment is performed under weak excitation condition, the TA intensity just after excitation is proportional to the excitation intensity and the decay remains unaffected by changes in the light intensity, suggesting geminate pair recombination. As will be shown later, the kinetics is highly nonexponential and shows a power law decay. The nonexponential decay of geminate pairs indicates that the recombination rate fluctuates according to the change in the distance between a pair owing to carrier movements. In Si-based semiconductors, the power law decay of luminescence was compared with the solution of diffusion equation under the influence of tunnelling recombination and the results show good agreements between them.[33] According to the theoretical results of diffusion-controlled geminate recombination, the density of geminate pairs decays by power law with the exponent given by 1/2.[33] As shown in Figure 5, the sub-microsecond decay observed for bare-LTON is consistent with the power law decay and the exponent is close to 1/2.

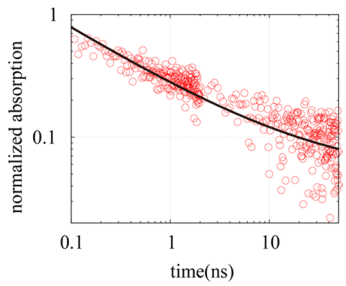

Figure 5. Nanosecond time profile for bare-LTON monitored at NIR (900−1500 nm) (λ_{exc} = 532 nm) and fitted curve to eqs 3 and 4. The (red) circles indicate the experimental results and the solid line is the fitted curve to eqs 3 and 4 (see the text for detailed fitting procedure).

By assuming the diffusional motion of carriers under Coulombic interaction between charged carriers, the density of geminate pairs having a separation r can be obtained by solving

$$\frac{\mathrm{d}}{\mathrm{d}t}\rho(r,t) = D\left[\frac{\partial^2}{\partial r^2}\rho(r,t) + \left(\frac{2}{r} + \frac{r_c}{r^2}\right)\frac{\partial}{\partial r}\rho(r,t)\right] - k(r)\rho(r,t) \quad (2)$$

where D denotes the mutual diffusion coefficient, and the intrinsic recombination rate is given by $k(r) = k_0\exp(-2br)$ using the inverse of the tunneling distance b, and the intrinsic rate k_0. $r_c = e^2/(4\pi\varepsilon\varepsilon_0 k_B T)$ denotes the Onsager distance, where ε, ε_0, k_B and T represent the relative dielectric constant, the vacuum permittivity, Boltzmann's constant and temperature. Previously, the equation was solved by prescribed diffusion approximation.[34,35] As pointed out by Shushin et al.,[35] the Coulombic interaction is taken into account perturbatively in the prescribed diffusion approximation and the approximation is not appropriate when the Coulombic attractive interaction is strongly characterized by the relative dielectric constant smaller than 10 and the intrinsic rate of tunnelling is small. The relative dielectric constant of LTON is assumed to be 8.91[36] and the intrinsic rate of tunnelling could be small to exhibit power law decay in nanosecond time scale. The strength of Coulombic interaction between oppositely charged carriers rapidly increases as the mutual distance decreases and the recombination kinetics depends crucially on the smallest separation distance.[37] We denote it by R and the perfectly reflecting boundary condition is set at R to solve eq 2. By applying perturbative expansion in terms of $k(r)$ using the known Green's function[38] we obtained the density of geminate pairs with the initial separation R as

$$S(t) = S_\infty + \frac{k_0}{D\sqrt{\pi D t}}\int_R^\infty \mathrm{d}r\, r^2 \exp\left(\frac{r_c}{r} - 2br\right) \quad (3)$$

where S_∞ is the ultimate survival density given by

$$S_\infty = 1 - \frac{k_0}{Dr_c}\int_R^\infty \mathrm{d}r\, r^2\left[\exp\left(\frac{r_c}{r}\right) - 1\right]\exp(-2br) \quad (4)$$

dx.doi.org/10.1021/ja5102823 | J. Am. Chem. Soc. 2014, 136, 17324−17331

Eq 3 can be derived even when the initial separation is larger than R by modifying S_∞. Regardless of the initial separation, the density of geminate pairs decays by power law with the exponent 1/2 by diffusion controlled tunneling recombination under Coulombic attractive interaction. In Figure 5, we show fitted decay profile of bare-LTON to eqs 3 and 4. The fitting procedure is as follows. First, by extracting the ultimate survival probability from the nanosecond time profile of the experimental results by assuming the power law decay, i.e., S_∞ = 0.047, we evaluate k_0/D with the aid of eq 4 by performing numerical integration with b = 1 nm^{-1}. Here we postulate that the smallest separation distance is R = 0.5 nm which corresponds to the typical lattice constant of semiconductors. Then, by fitting the experimental data to eq 3 with k_0/D = 4.47 × 10^{-3} nm^{-2} obtained in the previous step, we finally got D = 2.06 × 10^{-3} cm^2/s. By employing the value of the diffusion coefficient, we estimate the separation between carriers during the measurement time of 50 ns as 250 nm using $(6Dt)^{1/2}$. The relatively small value of the separation distance suggests that the effect of cocatalyst loading could be limited to carriers generated within the separation distance from the surface and most of carriers observed in our experiments are generated and decay in the bulk.

CONCLUSION

Using fs-TRDR spectroscopy we have successfully demonstrated trapped state sensitive kinetics in bare-LTON and 2 wt % CoO_x-LTON. Cocatalyst loading has an effect on the kinetics only when presence of excess energy (for above bandgap excitation) results in the generation of surface carriers. Thus, the kinetics also in turn depends on the choice of λ_{exc}. The observations and explanations bring forward some very interesting conclusions about the material such as there exists an energetic and spatial distribution of trapped carriers whose population is dependent on λ_{exc}. Excess energy in a way facilitates the migration of carriers to the surface and possibly this is the reason why in spite of having a band edge around 600 nm, LTON does not show appreciable activity toward the band edge. Moreover, when excited above bandgap (λ_{exc} = 480 nm), the results reveal trapping of surface holes in subpicosecond time scale (<1 ps) and nearly 30% surface electrons survive recombination at 2 ns in the presence of CoO_x. On the other hand, near bandgap excitation (λ_{exc} = 580 nm) results in slower decay of the less mobile deep trapped carriers thus, trapping in a way hinders the recombination loss. These carriers at later times may undergo detrapping and participate actively in photocatalytic reaction at the surface. Though, currently we have no such evidence. We have also investigated the decay of bulk carriers at nanosecond time scales. The slow decay was not affected by cocatalyst loading. The result suggests that the long-lived carriers are generated in the bulk. The decay was highly nonexponential and can be best fitted by a power law with the exponent of 1/2. The power law decay with this particular exponent can be obtained by the theory of diffusion controlled recombination of geminate pairs. By using the analytical formula for the density of geminate pairs, the diffusion coefficient was estimated. The bulk carriers could survive at sub-microsecond time range owing to the small intrinsic rate of recombination. However, the long-lived carriers decay even at sub-microsecond probably due to the small values of diffusion coefficients. Thus, we see that use of excess energy seems to results in the generation of surface holes and cocatalyst loading helps in their effective scavenging which is necessary for this n-type material to assist water oxidation. However, the small estimated value of diffusion coefficient indicates that it is difficult for most of the bulk carriers to reach to the surface of LTON. From experimental results and theoretical analysis, we conclude that since most of carriers in both the samples are generated in the bulk and are lost via geminate recombination, smaller sized particles possibly less than 250 nm (theoretically estimated separation distance between charge carriers at 50 ns) hold great potential for enhanced photocatalytic efficiency. As we have shown that the low value of diffusion coefficient is also a drawback for this material, better crystallinity may help in improving diffusion of charge carriers. Finally, we would like to emphasize once again that femtosecond transient absorption spectroscopy is a very efficient investigative tool to get such crucial information on the charge carrier kinetics in the primary stages of the photocatalysis process. This information can be utilized for the design of not only better quality LTON material in future, but in general such a knowledge is extremely beneficial for designing and synthesizing any photocatalytic material with improved performance, stability and reduced defect density.

ASSOCIATED CONTENT

Supporting Information

Excitation intensity dependence of the dynamics of the charge carriers, fs-TRDR spectra beyond 1000 nm, effect of addition of hole scavenger methanol on the decay of the photogenerated surface and bulk carriers in bare-LTON, femtosecond time profiles for bare-LTON and 2 wt % CoO_x-LTON monitored at 3440 nm (IR) for λ_{exc} = 480 nm. This material is available free of charge via the Internet at http://pubs.acs.org.

AUTHOR INFORMATION

Corresponding Authors

domen@chemsys.t.u-tokyo.ac.jp
akihiro-furube@aist.go.jp

Notes

The authors declare no competing financial interest.

ACKNOWLEDGMENTS

This work is supported by "Research Project for Future Development: Artificial Photosynthetic Chemical Process (ARPChem)" (METI/NEDO, Japan: 2012-2022).

REFERENCES

(1) Walter, M. G.; Warren, E. L.; McKone, J. R.; Boettcher, S. W.; Mi, Q.; Santori, E. A.; Lewis, N. S. *Chem. Rev.* **2010**, *110*, 6446−6473.
(2) Tachibana, Y.; Vayssieres, L.; Durrant, J. R. *Nat. Photonics* **2012**, *6*, 511−518.
(3) Osterloh, F. E. *Chem. Mater.* **2008**, *20*, 35−54.
(4) Maeda, K. *J. Photochem. Photobiol., C* **2011**, *12*, 237−268.
(5) Maeda, K. *Phys. Chem. Chem. Phys.* **2013**, *15*, 10537−10548.
(6) Moriya, Y.; Takata, T.; Domen, K. *Coord. Chem. Rev.* **2013**, *257*, 1957−1969.
(7) Kasahara, A.; Nukumizu, K.; Hitoki, G.; Takata, T.; Kondo, J. N.; Hara, M.; Kobayashi, H.; Domen, K. *J. Phys. Chem. A* **2002**, *106*, 6750−6753.
(8) Yashima, M.; Saito, M.; Nakano, H.; Takata, T.; Ogisu, K.; Domen, K. *Chem. Commun.* **2010**, *46*, 4704−4706.
(9) Maegli, A. E.; Pokrant, S.; Hisatomi, T.; Trottmann, M.; Domen, K.; Weidenkaff, A. *J. Phys. Chem. C* **2014**, *118*, 16344−16351.
(10) Zhang, F.; Yamakata, A.; Maeda, K.; Moriya, Y.; Takata, T.; Kubota, J.; Teshima, K.; Oishi, S.; Domen, K. *J. Am. Chem. Soc.* **2012**, *134*, 8348−8351.

(11) Minegishi, T.; Nishimura, N.; Kubota, J.; Domen, K. *Chem. Sci.* **2013**, *4*, 1120−1124.
(12) Matsukawa, M.; Ishikawa, R.; Hisatomi, T.; Moriya, Y.; Shibata, N.; Kubota, J.; Ikuhara, Y.; Domen, K. *Nano Lett.* **2014**, *14*, 1038−1041.
(13) Baxter, J. B.; Richter, C.; Schmuttenmaer, C. A. *Annu. Rev. Phys. Chem.* **2014**, *65*, 423−447.
(14) Furube, A.; Asahi, T.; Masuhara, H.; Yamashita, H.; Anpo, M. *J. Phys. Chem. B* **1999**, *103*, 3120−3127.
(15) Tamaki, Y.; Furube, A.; Murai, M.; Hara, K.; Katoh, R.; Tachiya, M. *J. Am. Chem. Soc.* **2006**, *128*, 416−417.
(16) Katoh, R.; Murai, M.; Furube, A. *Chem. Phys. Lett.* **2008**, *461*, 238−241.
(17) Tamaki, Y.; Hara, K.; Katoh, R.; Tachiya, M.; Furube, A. *J. Phys. Chem. C* **2009**, *113*, 11741−11746.
(18) Furube, A.; Maeda, K.; Domen, K. *Proc. SPIE* **2011**, *8109*, 810904−1−810904−8.
(19) Yamada, Y.; Sato, H. K.; Hikita, Y.; Hwang, H. Y.; Kanemitsu, Y. *Phys. Rev. Lett.* **2013**, *111*, 047403−047403−5.
(20) Barroso, M.; Stephanie R. Pendlebury, S. R.; Cowan, A. J.; Durrant, J. R. *Chem. Sci.* **2013**, *4*, 2724−2734.
(21) Fitzmorris, B. C.; Patete, J. M.; Smith, J.; Mascorro, X.; Adams, S.; Wong, S. S.; Zhang, J. Z. *ChemSusChem* **2013**, *6*, 1907−1914.
(22) Pendlebury, S. R.; Wang, X.; Formal, F. L.; Cornuz, M.; Kafizas, A.; Tilley, S. D.; Grätzel, M.; Durrant, J. R. *J. Am. Chem. Soc.* **2014**, *136*, 9854−9857.
(23) Furube, A.; Shiozawa, T.; Ishikawa, A.; Wada, A.; Domen, K.; Hirose, C. *J. Phys. Chem. B* **2002**, *106*, 3065−3072.
(24) Zhang, Y.; Tang, Y.; Liu, X.; Dong, Z.; Hng, H. H.; Chen, Z.; Sum, T. C.; Chen, X. *Small* **2014**, *9*, 996−1002.
(25) Tang, Y.; Jiang, Z.; Xing, G.; Li, A.; Kanhere, P. D.; Zhang, Y.; Sum, T. C.; Li, S.; Chen, X.; Dong, Z.; Chen, Z. *Adv. Funct. Mater.* **2013**, *23*, 2932−2940.
(26) Asahi, T.; Furube, A.; Fukumura, H.; Ichikawa, M.; Masuhara, H. *Rev. Sci. Instrum.* **1998**, *69*, 361−371.
(27) Yamanaka, K.; Morikawa, T. *J. Phys. Chem. C* **2012**, *116*, 1286−1292.
(28) Yamanaka, K.; Ohwaki, T.; Morikawa, T. *J. Phys. Chem. C* **2013**, *117*, 16448−16456.
(29) Kanan, M. W.; Nocera, D. G. *Science* **2008**, *321*, 1072−1075.
(30) Katoh, R.; Furube, A.; Fuke, N.; Fukui, A.; Koide, N. *J. Phys. Chem. C* **2012**, *116*, 22301−22306.
(31) Yamakata, A.; Kawaguchi, M.; Nishimura, N.; Minegishi, T.; Kubota, J.; Domen, K. *J. Phys. Chem. C* **2014**, *118*, 23897−23906.
(32) Yu, P. R.; Nedeljkovic, J. M.; Ahrenkiel, P. A.; Ellingson, R. J.; Nozik, A. J. *Nano Lett.* **2004**, *4*, 1089−1092.
(33) Hong, K. M.; Noolandi, J.; Street, R. A. *Phys. Rev. B: Condens. Matter Mater. Phys.* **1981**, *23*, 2967−2976.
(34) Seki, K.; Murayama, K.; Tachiya, M. *Phys. Rev. B: Condens. Matter Mater. Phys.* **2005**, *71*, 235212−1−235212−7.
(35) Shushin, A. I. *J. Chem. Phys.* **2008**, *129*, 114509−1−114509−11.
(36) Hisatomi, T.; Minegishi, T.; Domen, K. *Bull. Chem. Soc. Jpn.* **2012**, *85*, 647−655.
(37) Sano, H.; Tachiya, M. *J. Chem. Phys.* **1979**, *71*, 1276−1282.
(38) Lee, S.; Son, C. Y.; Sung, J.; Chong, S.-H. *J. Chem. Phys.* **2011**, *134*, 121102−1−121102−4.